Planetary and Space Science 266 (2025) 106179

Contents lists available at ScienceDirect

Planetary and Space Science

journal homepage: www.elsevier.com/locate/pss

Water-group ion irradiation studies of Enceladus ice analogues: Can radiolysis account for material in and around the south polar plume?

Grace Richards [a,*,1], Richárd Rácz [b], Sándor T.S. Kovács [b], Victoria Pearson [a], Geraint Morgan [a,2], Manish R. Patel [a], Simon Sheridan [a], Duncan V. Mifsud [b], Béla Sulik [b], Sándor Biri [b], Nigel J. Mason [b,c], Robert W. McCullough [d], Zoltán Juhász [b,**]

[a] School of Physical Sciences, The Open University, Milton Keynes MK7 6AA, United Kingdom
[b] HUN-REN Institute for Nuclear Research (Atomki), Debrecen H-4026, Hungary
[c] Physics and Astronomy, School of Engineering, Mathematics, and Physics, University of Kent, Canterbury, CT2 7NH, United Kingdom
[d] Department of Physics and Astronomy, School of Mathematics and Physics, Queen's University Belfast, Belfast, BT7 1NN, United Kingdom

ARTICLE INFO

Keywords:
Enceladus
Satellites
Surfaces
Ices
Infrared spectroscopy
Astrochemistry
Planetary science
Saturn
Magnetosphere

ABSTRACT

Saturn's magnetosphere contains trapped plasma and energetic charged particles which constantly irradiate the surface of Enceladus. In this study, we exposed Enceladean surface ice analogues containing H_2O, CO_2, CH_4, and NH_3 to water-group ions (e.g., O^+, O^{3+}, OH^+, and H_2O^+) having energies between 10 and 45 keV with the aim of exploring the chemical evolution of these ices and characterising the extent to which the surface material on Enceladus is weathered by Saturn's radiation environment. Each irradiation process was monitored *in situ* using Fourier-transform mid-infrared transmission absorption spectroscopy, and post-irradiative warming of the ices was performed to better characterise complex organic molecules formed as a result of the mobilisation of radiolytically generated radicals. Irradiation resulted in the formation of CO, OCN^-, and NH_4^+ in all experiments, and the radiolytic formation of formamide, acetylene, acetaldehyde, and hydroxymethyl radicals was also tentatively suggested in most experiments. Post-irradiative warming of the ices resulted in the formation of carbamic acid, ammonium carbamate, and an alcohol species. Although many of these products have not been previously observed on Enceladus' surface, some have been detected in Enceladus' plumes. Since our results demonstrate that the radiolytic formation of these molecules can occur over timescales similar to the exposure times of plume and surface material to magnetospheric radiation, questions must be raised as to whether such material originates directly from the subsurface ocean or is instead formed within the radiation-rich space environment.

1. Introduction

Enceladus is a prime candidate for future missions to investigate habitability in the outer Solar System (MacKenzie et al. 2021; Mousis et al. 2022; Martins et al. 2024), owing to its global liquid water subsurface ocean which may potentially host hydrothermal activity conducive to the emergence of life (Brown et al. 2006; Spencer et al. 2006; Hsu et al. 2015). Subsurface ocean material is ejected by plumes in the south polar region, and the majority of this material is deposited back onto the Enceladean icy surface (Brown et al. 2006; Kempf et al. 2010). The rapid resurfacing around the plume vents means that material of subsurface origin may not have been heavily processed by space weathering, and therefore could be used as a reliable indicator of the oceanic composition without needing to directly access the subsurface ocean (Jaumann et al. 2008; Kempf et al. 2010; Southworth et al. 2018; Franchi et al. 2025). However, if the surface composition of Enceladus around the plume vents is to be used as a proxy for better understanding the subsurface ocean environment, or even its potential habitability, then it is imperative for space weathering processes occurring on the icy surface of Enceladus and within its plumes to be fully understood so that

* Corresponding author.
** Corresponding author.
E-mail addresses: grace.richards@inaf.it (G. Richards), zjuhasz@atomki.hu (Z. Juhász).
[1] Present address: Istituto Nazionale di Astrofisica (INAF) – IAPS, Rome 00133, Italy.
[2] Present address: School of Chemistry and Chemical Engineering, University of Southampton, Southampton SO17 1BJ, United Kingdom.

https://doi.org/10.1016/j.pss.2025.106179
Received 29 April 2025; Received in revised form 2 July 2025; Accepted 18 July 2025
Available online 19 July 2025

they can be accommodated when interpreting observational data acquired from satellites.

The surface of Enceladus is known to host a complex radiation environment mediated by a number of sources, including galactic cosmic rays, high-energy protons sourced from the β-decay of neutrons themselves produced by cosmic ray interactions with the main Saturnian rings (Cooper, 1983), ions and electrons accelerated to keV-MeV energies by the Saturnian magnetosphere (Young et al. 2005), thermal ions and electrons (Barbosa, 1993, Ip, 2000), and solar ultraviolet photons. Prior experimental work seeking to constrain the physico-chemical effects of space weathering on the icy Enceladean surface have primarily made use of electrons (Hand and Carlson, 2011; Bergantini et al. 2014; Bramble and Hand, 2024) and ions (Strazzulla and Palumbo, 1998; Rachid et al. 2020); however, no prior study has yet considered the effects of so-called water-group ions (e.g., H_2O^+ or OH^+). This gap in the literature is somewhat striking, particularly since water-group ions are thought to comprise the bulk of the Saturnian magnetospheric ion population at the orbit of Enceladus, with keV H_2O^+ ions thought to account for upwards of 60 % of the ion population (Johnson et al. 2008; Paranicas et al. 2008; Tokar et al. 2008, 2009; Howett et al. 2018; Smith et al. 2018).

The importance of these water-group ions over other components of the magnetosphere, such as electrons, is further emphasised when considering the magnetic gyroradii of these charged particles. Ions with energies of a few tens of keV will have gyroradii of a few hundred kilometres, whereas electrons of the same energy will have significantly lower gyroradii of just a few tens of metres (Thomsen and Van Allen, 1980). This means that, while keV electrons will likely only impact the trailing hemisphere of Enceladus at lower latitudes, keV ions (especially water-group ions) are more likely to reach southern polar regions from upstream magnetospheric flows where they will act as the primary drivers of space weathering. Such space weathering may result in stark changes to the surface properties of Enceladus, and may have important implications for the surface chemistry occurring there. Observations by the Composite Infrared Spectrometer (CIRS) and the Imaging Science Subsystem (ISS) instruments aboard the *Cassini* mission revealed that on Saturn's inner satellites, such as Mimas and Tethys, irradiation by cold magnetospheric plasma results in a darkening of the ultraviolet-infrared reflectance spectra and produces 'bullseye'-shaped features on the moons' surfaces (Howett et al. 2018). However, on Enceladus, the physico-chemical effects of magnetospheric ion irradiation are significantly more difficult to determine because of the competing processes of E-ring grain bombardment and plume deposition (Paranicas et al. 2014).

Therefore, in an effort to better constrain the chemical transformations resulting from the magnetosphere-mediated space weathering of the surface environment of Enceladus in the south polar region where plume deposition rates are highest, we have performed experiments in which surface ice analogues composed of H_2O:CO_2:CH_4:NH_3 (approximate stoichiometry of 6:1:1:1) were exposed in an ultrahigh-vacuum set-up to water-group ion beams supplied by an electron cyclotron resonance ion source (ECRIS). This ice composition was selected based on the knowledge that the surface ice on Enceladus is primarily composed of H_2O, but also contains lower abundances (typically a few percent by weight) of volatile species such as CO_2, CH_4, and NH_3 (Emery et al. 2005; Brown et al. 2006; Hendrix et al. 2010; Villanueva et al. 2023). Irradiation experiments were carried out at 70 K, and radiation-induced chemical changes were analysed *in situ* using Fourier-transform mid-infrared (FTIR) absorption spectroscopy. Further details on our experimental methodology and apparatus are provided in Section 2, while our results and their applications to Enceladus are discussed in Sections 3 and 4, respectively. Finally, concluding remarks are given in Section 5.

2. Methods

Experiments were performed using the Atomki-Queen's University Ice Laboratory for Astrochemistry (AQUILA); an ultrahigh-vacuum laboratory set-up designed to study the effects of keV ion irradiation on astrophysical ice analogues at the HUN-REN Institute for Nuclear Research (Atomki) in Debrecen, Hungary. A detailed description of the AQUILA (Fig. 1) may be found in the work of Rácz et al. (2024), and so only the most salient details will be described here. Briefly, the AQUILA is an ultrahigh-vacuum chamber with base pressures of *circa* 5×10^{-9} mbar achieved through the combined use of three turbomolecular pumps backed by a scroll pump. Within the centre of the chamber is an oxygen-free high-conductivity copper sample holder into which a ZnSe deposition substrate is mounted. The sample holder and deposition substrate can be cooled down to 20 K by means of a closed-cycle helium cryostat; however, their temperature can be accurately regulated within the 20–300 K range by setting an equilibrium between the cooling effect of the cryostat and the warming induced by an internal cartridge heater.

Ices are prepared on the cooled deposition substrate by the background condensation of dosed gases and vapours. In the present experiments, CO_2, CH_4, and NH_3 gas samples were pre-mixed in a 1:1:1 ratio in a dosing line nominally held under vacuum. A separate dosing line contained water vapour that was sourced from a liquid sample that had been de-gassed through several freeze-pump-thaw cycles. Enceladus surface ice analogues were prepared at 20 K by co-depositing the gas and water vapour samples *via* their simultaneous introduction from the dosing lines into the main chamber. FTIR absorption spectra were acquired *in situ* during deposition to monitor the molecular compositions of the ices, which may differ from their compositions in the gas phase due to each molecular species being characterised by a different sticking coefficient to the cold substrate. The abundance of a particular species in an ice analogue was determined through its column density N (molecules cm^{-2}) by measuring the integrated absorbance S (cm^{-1}) of a characteristic mid-infrared absorption band. These two quantities are related as follows (Rácz et al. 2024):

$$N = \ln(10)\frac{S}{A_\nu} \tag{1}$$

where A_ν (cm molecule^{-1}) is the strength constant of the band. A list of absorbance bands and their associated strength constants used to quantify the composition of our Enceladean ice analogues is provided in Table 1. The average composition of the Enceladean ice analogues considered in this study was H_2O:CO_2:CH_4:NH_3 $\approx$ 6:1:1:1. It is to be noted that such ices are somewhat enriched in volatiles compared to what is actually expected on Enceladus; where CO_2, CH_4, and NH_3 respectively have $<$15, $<$7, and $<$3 percent by weight abundances on the surface (Emery et al. 2005; Brown et al. 2006; Hendrix et al. 2010; Combe et al. 2019). However, similar surface ice analogue compositions have been considered in previous studies (e.g., Bergantini et al. 2014; Rachid et al. 2020) so as to facilitate accurate spectroscopic analysis of the radiation-induced destruction of these volatiles and the synthesis of product molecules.

Once deposited to a desired thickness (i.e., $>$300 nm), ice deposition was ceased and the pressure levels within the AQUILA chamber were allowed to return to base level. The ices were subsequently warmed to 70 K, which is more representative of the mean Enceladean surface temperature (Spencer and Nimmo, 2013, and references therein). We note that our previous work has suggested that the structure and morphology of an ice is impacted by the temperature at which it is deposited, and that an ice prepared at a given cryogenic temperature will be more structurally ordered than one prepared by deposition at a lower temperature and then warmed to the given temperature (e.g., Mifsud et al. 2023a; Mifsud et al. 2024). Nevertheless, our present ice preparation methodology is advantageous in at least two ways. Firstly, it allows for highly volatile components of our Enceladean surface ice analogues, which may not condense as solids at 70 K, to be trapped within the growing ice structure by less volatile components during deposition at 20 K and thus be preserved within the ice as it is warmed to

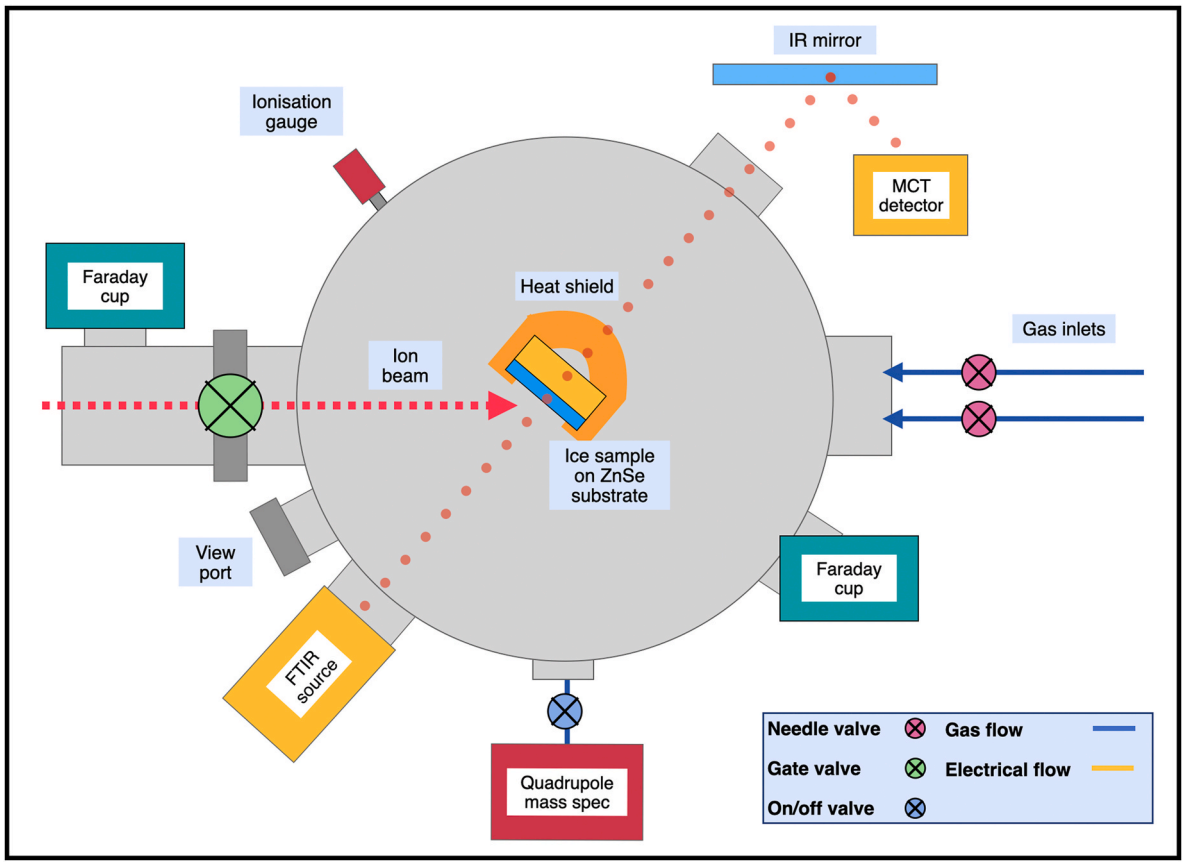

Fig. 1. Schematic diagram of the AQUILA chamber. See Rácz et al. (2024) for a more detailed description.

Table 1
List of mid-infrared bands and their associated strength constants used to quantify the composition of the Enceladean ice analogues considered in this study.

Molecule	Band Position (cm^{-1})	A_ν (cm $molecule^{-1}$)	References
H_2O	~3250	2.00×10^{-16}	Gerakines et al. (1995)
CO_2	2338	7.60×10^{-17}	Gerakines et al. (1995)
CH_4	1301	7.76×10^{-18}	Pearl et al. (1991)
NH_3	1110	1.70×10^{-17}	d'Hendecourt and Allamandola (1986)

Table 2
Summary of ice irradiation experiments performed as part of this study.

Ice Composition (H_2O:CO_2:CH_4:NH_3)	Ice Thickness (nm)	Projectile Ion	Total Irradiation Time (mins)	Total Irradiation Fluence (10^{16} cm^{-2})
4.5:1.9:1.5:2.1	329	10 keV O^+	68	1.70
5.4:1.8:1.4:1.4	373	45 keV O^{3+}	68	0.77
5.4:1.9:1.1:1.7	397	10 keV OH^+	148	1.46
5.7:1.9:0.7:1.6	388	15 keV OH^+	93	2.15
7.7:0.7:1.6:0.5	350	15 keV H_2O^+	48	2.11

higher temperatures. This is particularly true for the CH_4 component of the ices, which undergoes sublimation at temperatures well below 70 K under ultrahigh-vacuum conditions (Collings et al. 2004). Secondly, a less structurally ordered ice analogue mimics well the amorphous ice known to exist on Enceladus between the Tiger Stripe regions (Robidel et al. 2020), which is most likely formed either as a result of icy plume grains deposited around the stripes undergoing intense bombardment by high-energy particles deflected from Saturn's magnetosphere towards the south pole, or as a result of water vapour from the plumes rapidly condensing upon contact with the cold surface of the satellite (Newman et al. 2008).

At 70 K, the surface ice analogues were exposed to ion beams supplied by the Atomki ECRIS (Biri et al. 2012, 2021). In five separate experiments (summarised in Table 2), ices were irradiated by 10 keV O^+, 45 keV O^{3+}, 10 and 15 keV OH^+, and 15 keV H_2O^+ ions impacting the ice at an angle of 45° to the surface normal. Preliminary calculations performed using the *Stopping and Range of Ions in Matter* software package (Ziegler et al. 2010) showed that the maximum penetration range of each of these ions was significantly less than the >300 nm thickness of the ices, thus ensuring that each ion would implant within the ice as would be expected on the surface of Enceladus. Radiation-induced chemical changes in the ices were studied *in situ* using FTIR transmission absorption spectroscopy across the 4000-650 cm^{-1} wavenumber range at a nominal resolution of 2 cm^{-1}. Ices were irradiated until the main H_2O absorption peak was significantly depleted and did not seem to decrease further upon supplying greater ion fluences, with FTIR spectra being acquired at pre-selected fluence intervals. At the end of each irradiation experiment, the irradiated ices were warmed at a rate of 2 K min^{-1}, with FTIR spectra acquired at 10 K intervals. This post-irradiative warming was carried out with the intention of simulating the environment of (and, by extension, the thermally mediated chemistry within) the hot spots of the south polar regions of Enceladus from where the plumes emanate and where temperatures may be as high as 165 K (Brown et al. 2006; Spencer et al. 2006, 2009).

3. Results

Figs. 2–4 comprehensively summarise the results of our experiments. Fig. 2 depicts the FTIR spectra of the Enceladean surface ice analogues acquired before and after irradiation with each water-group ion, with all parent ice components labelled. More detailed band assignments for these parent ice species are also provided in Table 3. Fig. 3 exhibits the so-called 'difference spectra' obtained as a result of subtracting the spectrum of the ice prior to irradiation from that acquired after irradiation, which allow for radiolytic products to be more easily identified against the background continuum. Fig. 4 also shows difference spectra, only this time acquired as a result of subtracting the FTIR spectrum of an ice at the end of irradiation at 70 K from that acquired during post-irradiative warming at a temperature of 160 K. As such, these difference spectra allow for products formed thermally to be more easily identified. Assignments of the bands attributable to all products detected in our experiments are provided in Table 4.

3.1. Irradiation with 10 keV O^+ ions

Irradiation of the Enceladean surface ice analogue with 10 keV O^+ ions resulted in the rapid formation of CO, which was detected after a delivered fluence of just 4.13×10^{13} cm^{-2} through the observation of its characteristic stretching mode at 2137 cm^{-1} (Gerakines et al. 2023) in acquired FTIR spectra (Fig. 3). Additionally, a band located at 2167 cm^{-1} attributable to OCN^- (Hudson et al. 2001; van Broekhuizen et al. 2004) was also apparent in the spectra starting at fluences of about 2.88×10^{14} cm^{-2}. Lastly, a new band at 1490 cm^{-1} was observed starting at a fluence of 1.7×10^{16} cm^{-2}, which is most likely attributable to the formation of NH_4^+ (Frasco, 1964).

During post-irradiative warming of the ice, two new bands were observed in the spectra at 1538 and 1407 cm^{-1} beginning at a temperature of 130 K (Fig. 4). These bands are tentatively assigned to either carbamic acid (H_2NCOOH) or ammonium carbamate (NH_4^+ H_2NCOO^-), whose formation has been reported by previous studies concerned with the low-temperature thermal and irradiative processing of ices containing CO_2 and NH_3 (Khanna and Moore, 1999; Bossa et al. 2008; Jheeta et al. 2012; Potapov et al. 2020; James et al. 2020, 2021). Complimentary evidence of the formation of these species was found in the observation of the NH_4^+ band at 1490 cm^{-1}, which appeared during irradiation and became more intense during warming.

Once the ice had been warmed further to 150 K, a new peak at 1042

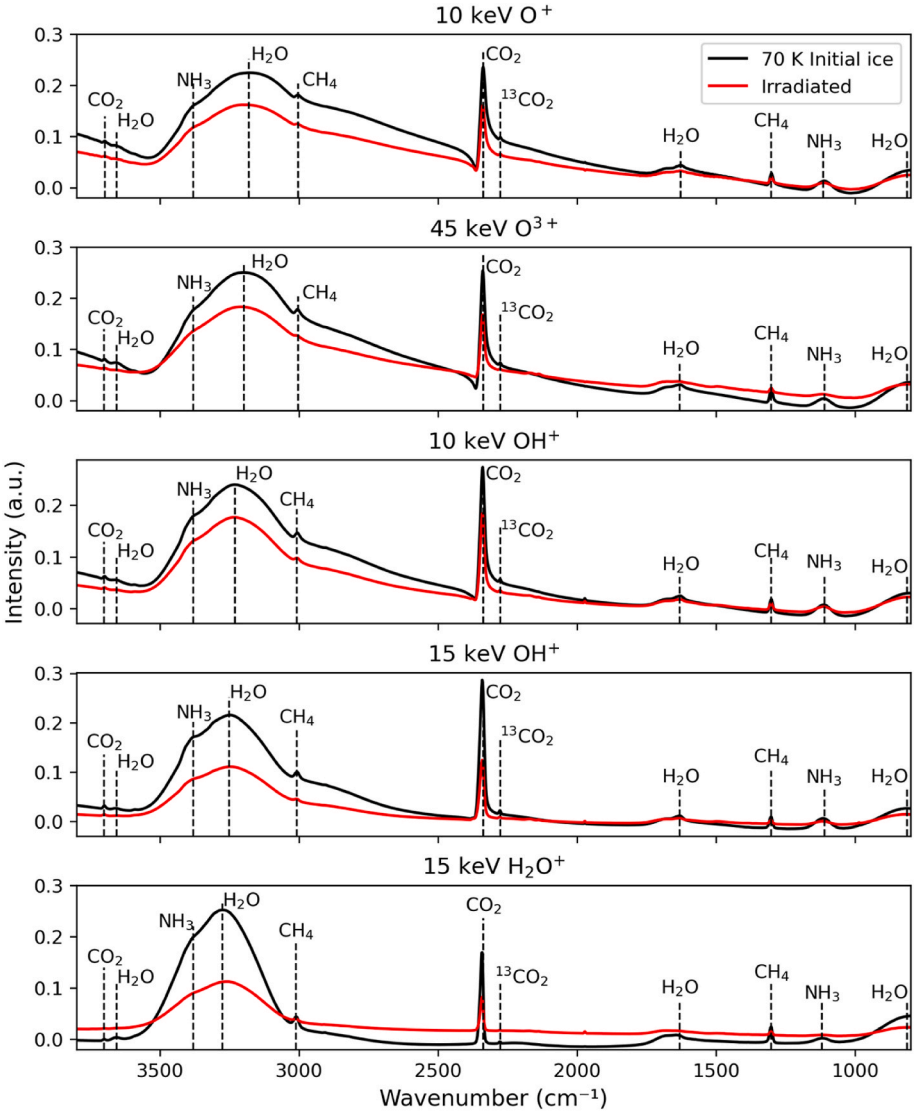

Fig. 2. FTIR spectra of the Enceladean surface ice analogues acquired prior to (black trace) and after (red trace) irradiation with different water-group ions at 70 K. Bands attributable to parent ice species (i.e., H_2O, CO_2, CH_4, and NH_3) are labelled, with further details on their main band positions given in Table 3. (For interpretation of the references to colour in this figure legend, the reader is referred to the Web version of this article.)

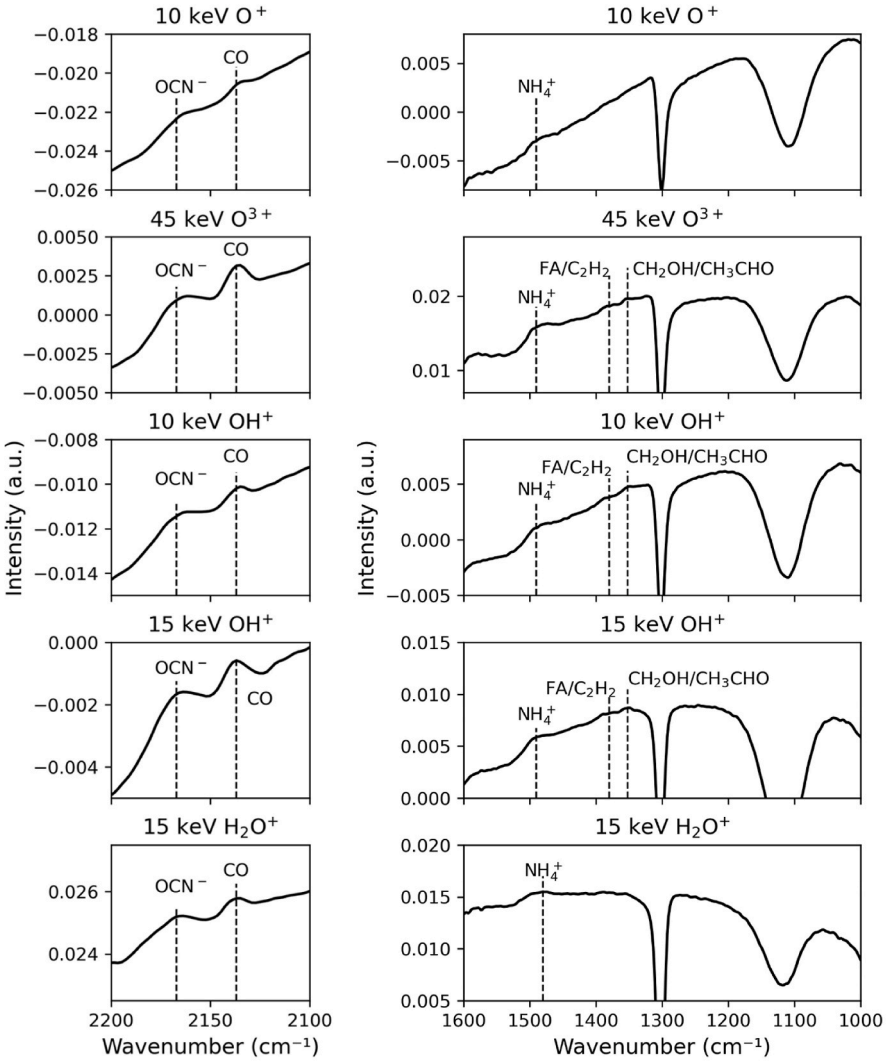

Fig. 3. FTIR difference spectra obtained by subtracting the spectrum of the Enceladean ice analogues acquired prior to irradiation from that acquired after irradiation using each water-group ion. These spectra better highlight the products formed as a result of irradiation. Note that FA refers to formamide.

cm^{-1} became apparent (Fig. 4). This band is coincident with the most intense absorption feature of O_3 (Chaabouni et al. 2000); however, we exclude O_3 as a likely carrier of this band in our experiments due to the known volatility of this species at 150 K under ultrahigh-vacuum conditions together with its known propensity to be efficiently destroyed by OH radicals, which should be efficiently produced in the irradiated ice. Instead, we propose that this absorption band is related to the C–O bond in one or more alcohol species (Zeiss and Tsutui, 1953). Although we cannot determine with any certainty which homologues are present, it is likely that simpler alcohols such as methanol (CH_3OH) and ethanol (CH_3CH_2OH) would be more abundant (Bergantini et al. 2014; Rachid et al. 2020). Finally, we note the emergence of an absorption feature at 1264 cm^{-1} at 150 K which we are unable to assign.

3.2. Irradiation with 45 keV O^{3+} ions

Similar to the irradiation experiment conducted with 10 keV O^+ ions, the irradiation using 45 keV O^{3+} ions resulted in the rapid synthesis of CO and OCN^- (Fig. 3), whose absorption features were visible in acquired FTIR spectra at 2137 and 2167 cm^{-1}, respectively (Hudson et al. 2001; van Broekhuizen et al. 2004; Gerakines et al. 2023). Other new bands were also observed during irradiation; most prominently those bands at 1380 and 1352 cm^{-1} (Fig. 3). The former of these bands is most likely associated with either acetylene (C_2H_2) (Hudson et al. 2014, Abplanalp and Kaiser, 2020) or formamide ($HCONH_2$) (Brucato et al. 2006; Sivaraman et al. 2013). In the case of the band at 1352 cm^{-1}, the most likely carriers are either hydroxymethyl radicals (CH_2OH) (Jacox and Milligan, 1973) or acetaldehyde (CH_3CHO) (Terwisscha van Scheltinga et al. 2018; Hudson and Ferrante, 2020). It is to be acknowledged that the stability of CH_2OH radicals at 70 K is questionable, and that it is likely that this band can be mostly attributed to CH_3CHO. However, we are unable to definitively exclude the presence of CH_2OH radicals in the irradiated ice. Indeed, given the difficulty in providing an unambiguous assignment for the FTIR absorption features at 1380 and 1352 cm^{-1}, the identifications of C_2H_2, $HCONH_2$, CH_2OH, and CH_3CHO in this experiment must be regarded as tentative.

During post-irradiative warming of the ice, a trio of bands at 1548, 1490, and 1407 cm^{-1} became increasingly apparent in the acquired spectra and were tentatively ascribed to the formation of carbamic acid or ammonium carbamate (Khanna and Moore, 1999; Bossa et al. 2008; Jheeta et al. 2012; Potapov et al. 2020; James et al. 2020, 2021), as was the case in the irradiation using 10 keV O^+ ions (Fig. 4). The band at 1490 cm^{-1} was visible even during irradiation (i.e., before warming began), starting at a fluence of 1.54×10^{14} cm^{-2}. This may be indicative

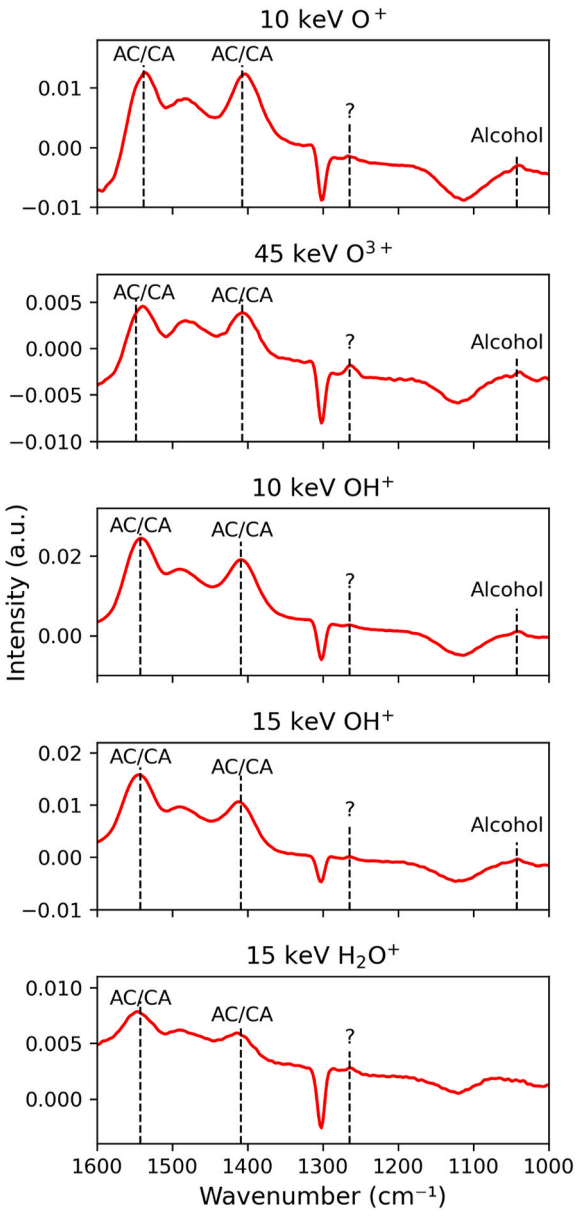

Fig. 4. FTIR difference spectra obtained by subtracting the spectrum of the Enceladean ice analogues acquired at the end of irradiation at 70 K from the spectrum of the ice during post-irradiative warming at 160 K. These spectra better highlight products that formed thermally in our experiments. Note that AC/CA refers to ammonium carbamate or carbamic acid.

of the formation of NH_4^+ ions within the ice as a result of the radiolysis-induced protonation of NH_3. Such a reaction has been observed in previous studies concerned with the irradiation of NH_3-containing ices (Moore et al. 2007; Moon et al. 2010). The post-irradiative warming of the ice also resulted in the formation of an absorption feature at 1042 cm^{-1} which, once again, was attributed to an alcohol species (Zeiss and Tsutui, 1953). Similar to the previous irradiation experiment, an unidentified band at 1264 cm^{-1} was formed during post-irradiative warming at a temperature of 150 K.

3.3. Irradiation with 10 keV OH^+ ions

The irradiation of the Enceladean surface ice analogue with 10 keV OH^+ ions resulted in the rapid formation of CO and OCN^- (Fig. 3), as observed through the appearance of bands at 2137 and 2167 cm^{-1} (Hudson et al. 2001; van Broekhuizen et al. 2004; Gerakines et al. 2023).

Table 3
Assignment of the absorption bands attributable to the parent ice species in the FTIR spectrum of the Enceladean surface ice analogues. Assignments were made with reference to previous studies by Hagen et al. (1981), Gerakines and Hudson (2015a), Gerakines and Hudson (2015b), and Hudson et al. (2022).

Molecule	Vibrational Mode	Band Position in FTIR Spectrum (cm^{-1})				
		10 keV O^+	45 keV O^{3+}	10 keV OH^+	15 keV OH^+	15 keV H_2O^+
CO_2	Combination	3698	3702	3702	3702	3701
H_2O	Dangling bonds	3656	3656	3656	3656	3656
NH_3	N–H bend	3380	3380	3380	3380	3380
H_2O	O–H stretch	3181	3198	3231	3251	3275
CH_4	C–H streth	3003	3003	3008	3008	3012
CO_2	C=O stretch	2337	2338	2338	2338	2338
$^{13}CO_2$	C=O stretch	2276	2276	2276	2276	2276
H_2O	O–H bend	1627	1631	1631	1631	1631
CH_4	C–H deformation	1302	1301	1301	1301	1301
NH_3	NH umbrella	1114	1110	1110	1110	1119
H_2O	Libration	813	813	813	825	813

Small absorption bands at 1380 and 1352 cm^{-1} associated with the tentative identifications of C_2H_2, $HCONH_2$, CH_2OH, and CH_3CHO also became visible during irradiation (Brucato et al. 2006; Sivaraman et al. 2013; Hudson et al. 2014, Abplanalp and Kaiser, 2020). Another band that appeared during irradiation was that at 1490 cm^{-1}, which could be detected starting from a fluence of 1.16 × 10^{16} cm^{-2} and which increased in intensity during post-irradiative warming (Fig. 4). This band has been attributed to NH_4^+, and its maximum intensity was recorded during warming at a temperature of 150 K. At this temperature, adjacent bands at 1542 and 1409 cm^{-1}, which were tentatively attributed to either ammonium carbamate or carbamic acid (Khanna and Moore, 1999; Bossa et al. 2008; Jheeta et al. 2012; Potapov et al. 2020; James et al. 2020, 2021), also reached their maximum intensity. During post-irradiative warming, a band at 1042 cm^{-1} was observed starting at a temperature of 140 K (Fig. 4), which we propose is associated with the formation of an alcohol species (Zeiss and Tsutui, 1953). Finally, an unidentified band at 1264 cm^{-1} was observed to appear at 150 K.

3.4. Irradiation with 15 keV OH^+ ions

As with the 10 keV OH^+ ion irradiation experiment, irradiation using 15 keV OH^+ ions resulted in the formation of CO and OCN^- (Fig. 3), as determined by the bands observed at 2137 and 2167 cm^{-1} (Hudson et al. 2001; van Broekhuizen et al. 2004; Gerakines et al. 2023). Additionally, a band at 1490 cm^{-1} became apparent starting at a fluence of 3.09 × 10^{14} cm^{-2} and increased in intensity during post-irradiative warming, reaching a maximum intensity at 140 K. Two more bands also appeared during warming at 1542 and 1409 cm^{-1} (Fig. 4); collectively, these three bands have been tentatively ascribed to NH_4^+ and ammonium carbamate or carbamic acid (Khanna and Moore, 1999; Bossa et al. 2008; Jheeta et al. 2012; Potapov et al. 2020; James et al. 2020, 2021). Furthermore, a band that could be tentatively assigned to either $HCONH_2$ or C_2H_2 at 1380 cm^{-1} and another that could be tentatively assigned to CH_2OH or CH_3CHO at 1352 cm^{-1}, were observed during both ion irradiation and warming (Brucato et al. 2006; Sivaraman et al. 2013; Hudson et al. 2014; Abplanalp and Kaiser, 2020). Post-irradiative warming also resulted in the development of an absorption feature at 1042 cm^{-1}, which has been tentatively assigned to an alcohol molecule (Zeiss and Tsutui, 1953). Finally, we note the emergence of an absorption band at 1264 cm^{-1} during warming at a temperature of 150 K which we were not able to assign.

Table 4
Formation of products as a result of the irradiation of Enceladean surface ice analogues with water-group ions and subsequent warming.

Molecule	Band Position in FTIR Spectrum (cm^{-1})					References
	10 keV O^+	45 keV O^{3+}	10 keV OH^+	15 keV OH^+	15 keV H_2O^+	
OCN^-	2167	2167	2167	2167	2167	Refs. [1,2]
CO	2137	2137	2137	2137	2137	Ref. [3]
H_2NCOOH or NH_4^+ H_2NCOO^-	1538[a]	1548[a]	1542[a]	1542[a]	1542[a]	Refs. [4–6]
NH_4^+	1490	1490	1490	1490	1480	Ref. [7]
H_2NCOOH or NH_4^+ H_2NCOO^-	1407[a]	1407[a]	1409[a]	1409[a]	1409[a]	Refs. [4–6]
$HCONH_2$ or C_2H_2	–	1380	1380	1380	–	Refs. [8–11]
CH_2OH or CH_3CHO	–	1352	1352	1352	–	Refs. [12–14]
?	1264[a]	1264[a]	1264[a]	1264[a]	1264[a]	–
Alcohol	1042[a]	1042[a]	1042[a]	1042[a]	–	Refs. [15–17]

Refs. [1–2]: Hudson et al. (2001); van Broekhuizen et al. (2004).
Ref. [3]: Gerakines et al. (2023).
Refs. [4–6]: Khanna and Moore (1999); Bossa et al. (2008); Jheeta et al. (2012).
Ref. [7]: Moore et al. (2007).
Refs. [8–11]: Brucato et al. (2006); Sivaraman et al. (2013); Hudson et al. (2014); Abplanalp and Kaiser (2020).
Refs. [12–14]: Jacox and Milligan (1973); Terwisscha van Scheltinga et al. (2018); Hudson and Ferrante (2020).
Refs. [15–17]: Zeiss and Tsutui (1953); Hudson (2017); Hudson et al. (2024).
[a] Band was only detected during post-irradiative warming of the ice.

3.5. Irradiation with 15 keV H_2O^+ ions

Similar to the experiment using 10 keV OH^+ ions, the irradiation of the Enceladean surface ice analogue with 15 keV H_2O^+ ions resulted in the appearance of fewer new peaks. Aside from CO and OCN^-, which were respectively observed through characteristic absorption bands at 2137 and 2167 cm^{-1} (Fig. 3), the only new band that was observed during irradiation was that at 1480 cm^{-1} attributed to NH_4^+, which could be observed only after a fluence of 2.11×10^{16} cm^{-2} had been delivered to the ice. During post-irradiative warming, new bands at 1542 and 1409 cm^{-1} were observed and were most prominent at 150 K (Fig. 4). These bands were associated with the formation of ammonium carbamate or carbamic acid. Moreover, an unidentified absorption band at 1264 cm^{-1} was observed during post-irradiative warming.

4. Discussion

4.1. Water-group ion irradiation of Enceladean surface ice analogues

The aim of this study was to better constrain the chemical transformations induced within the surface ices at the south polar region of Enceladus by magnetospheric water-group ions. To this end, we irradiated Enceladean surface ice analogues at 70 K using 10 keV O^+, 45 keV O^{3+}, 10 keV OH^+, 15 keV OH^+, and 15 keV H_2O^+ ions. Overall, the results obtained when using different projectile ions were qualitatively similar, with common products forming across different experiments. For instance, CO, OCN^-, and NH_4^+ were identified in all experiments (Table 4), while tentative detections of $HCONH_2$, C_2H_2, CH_2OH, and CH_3CHO were made in three of five experiments (Table 4). Moreover, post-irradiative warming of the ices also produced uniform results across projectile ion types, with ammonium carbamate or carbamic acid being detected in each experiment, along with an unidentified product exhibiting an absorption band at 1264 cm^{-1}. The observed formation of ammonium carbamate or carbamic acid in every experiment is consistent with the facile synthesis of these species in astrophysical environments containing CO_2 and NH_3 ices, as discussed in detail by Marks et al. (2023). An alcohol (likely CH_3OH or CH_3CH_2OH) was also produced during warming in all experiments except that making use of H_2O^+ ions (Table 4).

It is worth noting that no complex organic molecules were synthesised as a result of the irradiation of the Enceladean surface ice analogue by 15 keV H_2O^+ ions (Table 4). Such an observation is particularly interesting in light of the anticipated ubiquity of these ions in the south polar region of Enceladus, as discussed earlier. Although the exact reason for the non-detection of any radiolytic products other than CO, OCN^-, and NH_4^+ is not known, it is possible that this irradiation experiment was accompanied by more extensive sputtering due to the larger size of the projectile ion (Muntean et al. 2015), thus preventing the accumulation of complex product molecules. However, more detailed quantitative analyses are required in order to confirm this hypothesis. Such a rigorous quantitative analysis of our results would go beyond the scope of the present study; however, it is nonetheless worthwhile briefly comparing, in a qualitative manner, our results with those of previous laboratory studies on the irradiation of Enceladean surface ice analogues.

The key studies in this regard are those of Bergantini et al. (2014), which considered the 1 keV electron irradiation of a mixed ice composed of H_2O:CO_2:CH_4:NH_3:CH_3OH (in a compositional ratio of 100:13:4:3:2) at 20 K; and of Rachid et al. (2020), which considered the irradiation of a H_2O:CO_2:CH_4:NH_3 (10:1:1:1) mixed ice by both 108 keV O^{6+} and 15.7 MeV O^{5+} ions at 72 K. Comparing our results to those of these previous studies (Table 5), we find that there is a great overlap in the radiolytic species that could be spectroscopically identified. For example, all experiments detected CO and OCN^- among their radiolysis products; while NH_4^+, $HCONH_2$, CH_2OH, and CH_3CHO were identified in our present study as well as that of Bergantini et al. (2014). Indeed, unassigned bands at 1357, 1374, and 1385 cm^{-1} in the spectra of Rachid et al. (2020) may possibly be assigned to these products (Table 5). Although both our study and that of Bergantini et al. (2014) identify CH_2OH radicals as a radiolytic product, the identification is more questionable in our study due to the significantly greater temperature at which it was carried out compared to that of Bergantini et al. (2014), which should render these radicals highly unstable. That being said, Rachid et al. (2020) detected HCO radicals in their irradiated Enceladean ice analogue at 72 K, and so we cannot definitively exclude the presence of CH_2OH in our study. We also note that a band observed at 1484 cm^{-1} by Rachid et al. (2020) during the irradiation of their Enceladean surface ice analogue with 15.7 MeV O^{5+} ions was likely incorrectly assigned to H_2CO. We propose that the correct assignment is to NH_4^+.

Rachid et al. (2020) also observed the emergence of a band at 1015 cm^{-1} during the irradiation of their ice with 15.7 MeV O^{5+} ions, which they assigned to CH_3OH. This is broadly consistent with our assignment of a band at 1042 cm^{-1} that emerged during post-irradiative warming to an alcohol species, although we cannot propose which homologue is present with any certainty. Although it is likely that a simple alcohol (such as CH_3OH) is indeed the dominant contributor to this band, we note that the wavenumber position of this band in our experiment is somewhat intermediate the expected C–O stretching modes in the

Table 5
Qualitative comparison of the products obtained as a result of the irradiation of Enceladean surface ice analogues by this and previous studies. Note that the irradiations performed by Bergantini et al. (2014), Rachid et al. (2020), and this study were respectively carried out at 20, 72, and 70 K.

Bergantini et al. (2014) (1 keV e^-)		Rachid et al. (2020) (108 keV O^{6+})		Rachid et al. (2020) (15.7 MeV O^{5+})		This Study (45 keV O^{3+})	
Band Position (cm^{-1})	**Assignment**	**Band Position (cm^{-1})**	**Assignment**	**Band Position (cm^{-1})**	**Assignment**	**Band Position (cm^{-1})**	**Assignment**
–	–	–	–	1015	CH_3OH	1042[a]	Alcohol
1250	HMT[b]	–	–	–	–	1264[a]	?
1352	CH_2OH or CH_3CHO	–	–	1357	?	1352	CH_2OH[b] or CH_3CHO[b]
1383	$HCONH_2$	1374	?	1385	?	1380	$HCONH_2$[b] or C_2H_2[b]
–	–	–	–	–	–	1407[a]	AC or CA
1480	NH_4^+ or alkane	–	–	1484	H_2CO[b]	1490	NH_4^+
1500	NH_4^+ or H_2CO	–	–	–	–	–	–
–	–	–	–	–	–	1548[a]	AC or CA
1580	Carboxylate	–	–	–	–	–	–
–	–	–	–	1855	HCO	–	–
–	–	–	–	2045	CO_3	–	–
–	–	–	–	2089	CN^-	–	–
–	–	–	–	2097	HCN	–	–
2140	CO	2137	CO	2137	CO	2137	CO
2170	OCN^-	2171	OCN^-	2171	OCN^-	2167	OCN^-
–	–	–	–	2263	HNCO[b]	–	–

[a] Band was only detected in this study during post-irradiative warming of the ice.
[b] These products were only tentatively identified in their respective experiments.

spectra of neat CH_3OH and neat CH_3CH_2OH (Hudson, 2017; Hudson et al. 2024), suggesting at least some contribution from the latter species. Therefore, it is not possible to specify which alcohol species is present in our experiment as a radiolytic product.

In examining Table 5, it is possible to note that certain radiolytic products observed by Bergantini et al. (2014) or Rachid et al. (2020) were not observed in our study. In the case of Bergantini et al. (2014), these are mainly organic species (e.g., H_2CO, carboxylates, and hexamethylenetetramine) whose presence can be rationalised by the fact that this particular experiment initially included CH_3OH in the parent ice which could have served as a feedstock from which other organic species could be synthesised. In the case of Rachid et al. (2020), however, several simple molecular species could be identified as a result of the processing of their Enceladean surface ice analogue by 15.7 MeV O^{5+} ions, including CO_3, CN^-, HCN, and isocyanic acid (HNCO). These species were not identified as products in the present study. We speculate that the reason for this is related to the higher energy of the projectile ion used by Rachid et al. (2020), since previous experimental evidence has suggested that more energetic projectiles may indeed yield a greater diversity and abundance of products in an irradiated astrophysical ice analogue (e.g., Loeffler et al. 2005; Ding et al. 2013; Islam et al. 2014; Muñoz Caro et al. 2014; Mifsud et al. 2023b). It is therefore possible that these species were also produced in our experiment, but at concentrations that were too low to be detectable in acquired spectra.

Finally, it is necessary to address the relevance of the composition of our Enceladean surface ice analogues to the actual surface composition of Enceladus. As noted previously, the surface of Enceladus is composed overwhelmingly of H_2O ice with lower quantities of CO_2, CH_4, and NH_3 having been detected at abundances of <15, <7, and <3 percent by weight, respectively (Emery et al. 2005; Brown et al. 2006; Hendrix et al. 2010; Combe et al. 2019). As such, our surface ice analogues are somewhat enriched in these volatile species compared to the surface composition of Enceladus. However, it is important to note that the experiment of Bergantini et al. (2014) considered an Enceladean surface ice analogue whose composition closely mirrored that of the actual surface of Enceladus, and that the radiation chemistry and radiolytic product formation observed by Bergantini et al. (2014) are very similar to those observed in the present study (Table 5). The high degree of similarity between our present results and those obtained by experiments closely mimicking the surface composition of Enceladus (Bergantini et al. 2014) therefore validates our experiments and demonstrates that the radiation chemistry described herein and, by extension, the inferences drawn from this chemistry are applicable to the surface conditions of Enceladus. The remainder of this discussion is therefore dedicated to detailing the reaction network initiated by the irradiation of the Enceladean ice analogues considered in this study, and the implications of this radiation chemistry for the surface evolution of Enceladus, particularly in the south polar region.

4.2. Radiation chemistry

The three most commonly observed species in the ion irradiation experiments performed in this study were CO, OCN^-, and NH_4^+. The most likely synthesis route for CO is the radiation-induced homolytic dissociation of a C=O bond in CO_2 (Raut and Baragiola, 2013; Martín-Doménech et al. 2015; Mifsud et al. 2022). The synthesis of OCN^- is somewhat more complex, and most likely relies on the primary synthesis of HNCO, which then undergoes an acid-base reaction with either H_2O or NH_3 to yield the OCN^- product (Hudson et al. 2001; van Broekhuizen et al. 2004). Interestingly, this latter reaction also yields NH_4^+, and could account for a fraction of the NH_4^+ observed in our experiments:

$$NH_3 \xrightarrow{rad.} NH_2 + H \quad (2)$$

$$NH_2 + CO \rightarrow HNCO + H \quad (3)$$

$$HNCO + H_2O \text{ (or } NH_3) \rightarrow OCN^- + H_3O^+ \text{ (or } NH_4^+) \quad (4)$$

We note that no FTIR evidence for the formation of HNCO was found in our experiments, although this species was identified as a product by Rachid et al. (2020) during their irradiation of an Enceladean surface ice analogue by 15.7 MeV O^{5+} ions. It is therefore possible that this species was rapidly consumed upon production to yield the OCN^- product observed in our experiments and, indeed, previous work by van Broekhuizen et al. (2004) determined that the conversion of HNCO to OCN^- in the presence of NH_3 within an energetic environment is extremely efficient. Radiation-induced ionisation within the ice could also set the stage for ion-molecule reactions that could contribute to the abundance of NH_4^+, as discussed by Moore et al. (2007):

$$H_2O \text{ (or } NH_3) \xrightarrow{rad.} H_2O^+ \text{ (or } NH_3^+) + e^- \quad (5)$$

$$H_2O^+ \text{ (or } NH_3^+) + NH_3 \rightarrow OH \text{ (or } NH_2) + NH_4^+ \quad (6)$$

$$H_3O^+ + NH_3 \rightarrow H_2O + NH_4^+ \quad (7)$$

Beyond these three product molecules, all other detections in our experiments must be considered tentative. Among these tentative detections was the formation of an alcohol species, which was detected in all experiments except that making use of 15 keV H_2O^+ ions. Although we cannot unambiguously determine which alcohol homologues were present as products, it is likely that simpler alcohols such as CH_3OH and CH_3CH_2OH were more abundant than larger homologues. The most likely synthesis route towards the formation of CH_3OH is that discussed by Hodyss et al. (2009) for irradiated ices containing both CH_4 and H_2O:

$$H_2O \xrightarrow{rad.} H + OH \quad (8)$$

$$CH_4 + H\ (\text{or } OH) \rightarrow CH_3 + H_2\ (\text{or } H_2O) \quad (9)$$

$$CH_3 + OH \rightarrow CH_3OH \quad (10)$$

Since CH_3CH_2OH is a more complex molecule, multiple reaction pathways could have contributed to its synthesis in our irradiated Enceladean ice analogues. For instance, one pathway is analogous to that described by Eqs. (8)–(10), but starting from ethane (C_2H_6) rather than CH_4 (Moore and Hudson, 1998; de Barros et al. 2016; Mejía et al. 2020):

$$C_2H_6 + H\ (\text{or } OH) \rightarrow CH_3CH_2 + H_2\ (\text{or } H_2O) \quad (11)$$

$$CH_3CH_2 + OH \rightarrow CH_3CH_2OH \quad (12)$$

Ethane itself is readily produced as a result of the radiolysis of CH_4 (Bennett et al. 2006; de Barros et al. 2011; Vasconcelos et al. 2017), and thus could have been present within our ices at levels below spectroscopic detection limits. Another product of CH_4 radiolysis is C_2H_2 (Bennett et al. 2006; de Barros et al. 2011; Vasconcelos et al. 2017), which was also tentatively detected in a number of our experiments (Fig. 3, Table 4). This species may take part in radical addition reactions with OH and H to progressively saturate the carbon skeleton and finally yield CH_3CH_2OH (Chuang et al. 2020, 2021):

$$C_2H_2 + H\ (\text{or } OH) \rightarrow CH_2CH\ (\text{or } CHCHOH) \quad (13)$$

$$CH_2CH + OH\ (\text{or } CHCHOH + H) \rightarrow CH_2CHOH \xrightarrow{+H} CH_3CHOH \text{ or } CH_2CH_2OH \xrightarrow{+H} CH_3CH_2OH \quad (14)$$

Another possible route towards the formation of CH_3CH_2OH begins with the CH_3OH product itself, which may be dehydrogenated to CH_2OH radicals as a result of the impinging ionising radiation (Bergantini et al. 2017, 2018). This radical product was tentatively detected in three of our experiments (Fig. 3, Table 4). Subsequent methylation of the CH_2OH radical would yield CH_3CH_2OH:

$$CH_3OH \xrightarrow{rad.} CH_2OH + H \quad (15)$$

$$CH_3 + CH_2OH \rightarrow CH_3CH_2OH \quad (16)$$

The synthesis of vinyl alcohol (CH_2CHOH) as per Eq. (14) could also lead to the eventual formation of CH_3CHO, which was tentatively detected in the experiment making use of 45 keV O^{3+} ions, as well as those making use of 10 and 15 keV OH^+ ions. An input of energy in the form of ionising radiation could result in the removal of two hydrogen atoms from vinyl alcohol to yield ketene (H_2CCO) which can then be re-hydrogenated to produce CH_3CHO (Hudson and Loeffler, 2013; Chuang et al. 2021):

$$CH_2CHOH \xrightarrow{rad.} H_2CCO + 2\ H\ (\text{or } H_2) \quad (17)$$

$$H_2CCO + 2\ H \rightarrow CH_3CHO \quad (18)$$

Another tentative product observed in our irradiated ices was $HCONH_2$ (Fig. 3, Table 4). This product was observed in all experiments, apart from those using 10 keV O^+ ions and 15 keV H_2O^+ ions. The most probable synthetic route for this species is that suggested by Jones et al. (2011):

$$H + CO \rightarrow HCO \quad (19)$$

$$HCO + NH_2 \rightarrow HCONH_2 \quad (20)$$

Finally, we detected carbamic acid and ammonium carbamate during post-irradiative warming of all our Enceladean surface ice analogues (Fig. 4, Table 4). The synthesis of these species as a result of the irradiative or thermal processing of ices initially containing CO_2 and NH_3 has been described in detail by several previous studies (Bossa et al. 2008; Potapov et al. 2020; James et al. 2020, 2021; Marks et al. 2023). The mechanism leading to the formation of these products begins with Eq. (2), which yields NH_2 and H; the latter species reacting with CO_2 to yield COOH. The reaction between COOH and NH_2 then goes on to yield carbamic acid:

$$H + CO_2 \rightarrow COOH \quad (21)$$

$$COOH + NH_2 \rightarrow NH_2COOH \quad (22)$$

The acid-base reaction between carbamic acid and NH_3 then yields ammonium carbamate:

$$NH_2COOH + NH_3 \rightarrow NH_4^+NH_2COO^- \quad (23)$$

4.3. Surface evolution of Enceladus

As explained previously, the water-group ions used in this study are of particular relevance to Enceladus' south polar region, since their sheer abundance (Tokar et al. 2009) and comparatively high magnetic gyroradii (Thomsen and Van Allen, 1980) mean they are likely the primary drivers of radiolytic processing (i.e., space weathering) at the south polar region where subsurface ocean material is ejected *via* plumes and deposited onto the surface. Of these ions, H_2O^+ is probably the most important as it constitutes over 60 % of the total magnetospheric ion population (Tokar et al. 2009). However, if the influence of space weathering on the surface evolution of Enceladus is to be truly constrained, then it is necessary to first understand the production timescales of various radiolytic products in both the surface ices and the plumes (both of which are exposed to magnetospheric radiation) and the implications of such timescales for distinguishing material of subsurface oceanic origin from material produced by radiolytic processes at the surface and near-surface environments. The results of our present experiments suggest that CO, OCN^-, and NH_4^+, possibly together with carbamic acid and ammonium carbamate, are the most plausible species that are present on Enceladus as undetected surface constituents and the remainder of our discussion will therefore largely focus on these species.

4.3.1. Production timescales on the surface

The ion density around Enceladus has been reported to be approximately 60 cm^{-3}, with mean ion velocities of 32.7 km s^{-1} (Tokar et al. 2008; Persoon et al. 2013; Howett et al. 2018). The ion flux at the surface of Enceladus may be approximated as the product of these

quantities, and may thus be taken to be about 2×10^{12} m^{-2} s^{-1}. As such, the fluences used in the experiments presented here correspond to fluences of magnetospheric ions delivered to the surface of Enceladus over timescales of approximately 1–4 years.

The exposure time of surface material in areas with the highest rates of plume material deposition in the south polar region where burial of surface material occurs at a rate of 1 mm $year^{-1}$ (Southworth et al. 2018) is estimated to be about 1 year (Hendrix and House, 2023). The Enceladean timescales simulated by our experiments are therefore approximately equal to the exposure time of material around the south polar plumes, meaning that it would be very challenging to discriminate between a potentially oceanic or space weathering source for CO, OCN^-, and NH_4^+ detected in these regions. Moreover, our experiments demonstrate that these three products could be formed at relatively low ion fluences of about 10^{14} cm^{-2}, which correspond to timescales of just 6 days on the surface of Enceladus. This further complicates the search for an unambiguous source of CO, OCN^-, or NH_4^+ should they eventually be detected in surface material around the south polar plume. However, in regions characterised by significantly lower rates of plume material deposition, such as the northern hemisphere of Enceladus where surface burial rates are on the order of 10^{-4} mm $year^{-1}$, surface exposure timescales are well in excess of 1000 years. Consequently, in these regions, the chemical evolution of surface material is more likely to be driven by space weathering processes than by the deposition of plume material.

It should be noted that the calculated Enceladean surface timescales corresponding to the fluences used in our experiments are likely somewhat of an underestimate, since the ion density used in those calculations included the entire population around Enceladus rather than the individual ion species used in each of our experiments. Taking H_2O^+ as an example, which makes up about 60 % of the ion population around Enceladus (Tokar et al. 2009) and scaling the ion density accordingly, it is possible to calculate an Enceladean timescale of 6 years for a total experimental fluence of 2.11×10^{16} cm^{-2}. Although this is slightly longer than our initial estimate of 1–4 years, it is still on the same order of magnitude as surface exposure ages in regions where plume material deposition rates are high.

4.3.2. Production timescales in the plumes

Although none of the radiolytic product species observed in our experiments have been directly detected on the surface of Enceladus, many have actually been tentatively detected within its plumes. These species include CO, C_2H_2, and alcohols such as CH_3OH and CH_3CH_2OH (Postberg et al. 2018; Peter et al. 2024). The plumes, which are sourced from the subsurface ocean (Brown et al. 2006), also contain the molecules used to form our Enceladean surface ice analogues; i.e., H_2O, CO_2, CH_4, and NH_3 (Waite et al. 2017). The Saturnian magnetospheric plasma also interacts with (and, indeed, is partially composed of) this plume material. As such, and similarly to the surface ice material, the plume itself is also subject to radiation-driven chemistry (Tokar et al. 2009). Ion densities in the plume are actually thought to be higher than those at the surface of Enceladus: the Radio and Plasma Wave Science (RPWS) Langmuir probe aboard the *Cassini* mission measured maximum ion densities of 10^5 cm^{-3}, with ions having velocities ranging between 5 and 10 km s^{-1} (Morooka et al. 2011). However, lower mean ion densities of 400–900 cm^{-3} have been suggested on the basis of numerical models (Sakai et al. 2016).

Therefore, if our experiments were used to simulate the radiation-driven chemistry occurring within plume material rather than in the surface ices, then the fluences delivered in the present experiments would be delivered to the material within the plume in just 21–60 h if using the maximum measured ion densities (Morooka et al. 2011), or in 0.6–1.7 years if using the more conservative values suggested by models (Sakai et al. 2016). Assuming a typical launch velocity of 148 m s^{-1} and an average plume height of 400–700 km (Sharma et al. 2023), it is possible to estimate that a particle resides in the plume for 45–80 h. Therefore, our experiments are appropriate for simulating radiation-driven chemistry within the plume if the maximum magnetospheric ion fluxes are assumed to be correct. As such, it is not possible to discount radiation-driven chemistry as a source of molecules either in the plume or on the surface.

4.3.3. Implications for the origins of Enceladean surface ice constituents

Our experiments have therefore demonstrated that radiation in the form of Saturn's magnetospheric plasma may be a driver of chemistry leading to the formation of a number of new molecules over short timescales both on the surface of Enceladus as well as within its plumes. As such, it is likely that the composition of the subsurface ocean may not be accurately reflected by the composition of the emergent plume, or by material deposited on the surface immediately adjacent to the plume. This result may be of crucial importance when interpreting data from future missions to Enceladus (e.g., the proposed *Orbilander* and *Moonraker* missions; MacKenzie et al. 2021; Mousis et al. 2022) or when feeding data into models simulating the composition and chemistry of Enceladus' subsurface ocean. Moreover, a number of molecules detected (or tentatively detected) in our study may be candidates to constrain the habitability of Enceladus due to their known roles in prebiotic chemistry: for instance, $HCONH_2$ is a known chemical precursor to amino acids and nucleobases (Saladino et al. 2012; Ferus et al. 2015; López-Sepulcre et al. 2019), while phosphate derivatives of carbamic acid and ammonium carbamate are known participants in the biological urea cycle (Morris, 1992). Given that the downward transport of molecular material at the surface to the subsurface ocean is thought to occur over a timescale of at least a few millions or even a few tens of millions of years (Porco et al. 2006; Barr, 2008; Cooper et al. 2009), our results suggest that abiotic, radiation-driven processes may conceivably lead to the formation of prebiotic molecules under conditions relevant to the surface and plumes of Enceladus. Indeed, if such molecules are themselves radio-resistant or are preserved *via* burial beneath deposited plume ejecta, then it may be possible for them to accumulate on the surface and reach abundances that would be detectable by scientific instruments aboard future missions. Therefore, it may be necessary for caution to be adopted should future detections of these prebiotic species be interpreted as possible indicators of extant metabolic processes in Enceladus' subsurface ocean.

5. Conclusions

Experiments were performed in which Enceladean surface ice analogues were exposed to keV water-group ions (i.e., O^+, O^{3+}, OH^+, and H_2O^+) at 70 K so as to simulate the magnetosphere-driven radiation chemistry occurring at Enceladus' south polar region, where plumes eject subsurface ocean material which is then deposited on the icy surface. Our results demonstrated that the irradiation of these ices yielded a number of products, including CO, OCN^-, and NH_4^+, while post-irradiative warming resulted in the synthesis of carbamic acid and ammonium carbamate. Moreover, other organic molecules (e.g., C_2H_2, CH_3CHO, $HCONH_2$, CH_2OH, and an alcohol species) were tentatively detected. Although none of these products has yet been detected on the icy surface of Enceladus, some have actually been detected within its plumes. Importantly, our results have demonstrated that the timescales required to synthesise these products (some of which are considered prebiotic molecules) are similar to both the surface exposure times in regions of highest plume material deposition, as well as the residence time of material within the plume itself. Consequently, in such regions, it may be very challenging to discriminate material sourced from the subsurface ocean from that which is produced as a result of the exposure of material to radiation in the form of Saturn's magnetospheric plasma. Therefore, caution is advised if interpreting future detections of prebiotic molecules on Enceladus' south polar surface or within its plumes as evidence of life-driven processes occurring within the subsurface ocean.

CRediT authorship contribution statement

Grace Richards: Writing – review & editing, Writing – original draft, Resources, Project administration, Methodology, Investigation, Funding acquisition, Formal analysis, Data curation, Conceptualization. **Richárd Rácz:** Supervision, Software, Methodology, Investigation, Formal analysis, Data curation. **Sándor T.S. Kovács:** Software, Methodology, Investigation, Formal analysis, Data curation. **Victoria Pearson:** Writing – review & editing, Supervision, Funding acquisition, Conceptualization. **Geraint Morgan:** Writing – review & editing, Supervision. **Manish R. Patel:** Writing – review & editing, Supervision. **Simon Sheridan:** Supervision. **Duncan V. Mifsud:** Writing – review & editing, Writing – original draft, Validation, Methodology, Formal analysis, Conceptualization. **Béla Sulik:** Project administration, Methodology, Investigation, Funding acquisition, Data curation. **Sándor Biri:** Methodology, Investigation, Formal analysis, Data curation. **Nigel J. Mason:** Writing – review & editing, Project administration, Funding acquisition. **Robert W. McCullough:** Writing – review & editing. **Zoltán Juhász:** Writing – review & editing, Validation, Supervision, Resources, Project administration, Methodology, Investigation, Funding acquisition, Formal analysis, Data curation, Conceptualization.

Declaration of competing interest

The authors declare that they have no known competing financial interests or personal relationships that could have appeared to influence the work reported in this paper.

Acknowledgements

Comments and suggestions from two anonymous referees which helped to improve our manuscript are gratefully acknowledged. The authors acknowledge support from the Europlanet 2024 RI which has been funded by the European Union's Horizon 2020 Research and Innovation Programme under grant agreement no. 871149. This study is also based on work from the COST Actions CA20129 MultIChem and CA22133 PLANETS, supported by COST (European Cooperation in Science and Technology). Grace Richards is grateful for doctoral funding from the Research England 'Expanding Excellence in England' fund (grant code 124.18). Zoltán Juhász acknowledges support from the Hungarian Academy of Sciences in the form of a János Bolyai Research Scholarship.

Data availability

Data will be made available on request.

References

Abplanalp, M.J., Kaiser, R.I., 2020. Astrophys. J. 889 (3). https://doi.org/10.3847/1538-4357/ab616c.
Barbosa, D.D., 1993. J. Geophys. Res.: Space Phys. 98, 9335–9343. https://doi.org/10.1029/93JA00478.
Barr, A.C., 2008. J. Geophys. Res.: Planets 113, E07009. https://doi.org/10.1029/2008JE003114.
Bennett, C.J., Jamieson, C.S., Osamura, Y., Kaiser, R.I., 2006. Astrophys. J. 653, 792–811. https://doi.org/10.1086/508561.
Bergantini, A., Pilling, S., Nair, B.G., Mason, N.J., Fraser, H.J., 2014. Astron. Astrophys. 570, A120. https://doi.org/10.1051/0004-6361/201423546.
Bergantini, A., Maksyutenko, P., Kaiser, R.I., 2017. Astrophys. J. 841, 96. https://doi.org/10.3847/1538-4357/aa7062.
Bergantini, A., Góbi, S., Abplanalp, M.J., Kaiser, R.I., 2018. Astrophys. J. 852, 70. https://doi.org/10.3847/1538-4357/aa9ce2.
Biri, S., Rácz, R., Pálinkás, J., 2012. Rev. Sci. Instrum. 83, 02A341. https://doi.org/10.1063/1.3673006.
Biri, S., Vajda, I.K., Hajdu, P., Rácz, R., Csík, A., Kormány, Z., Perduk, Z., Kocsis, F., Rajta, I., 2021. European Phys. J. Plus 136, 247. https://doi.org/10.1140/epjp/s13360-021-01219-z.
Bossa, J.B., Theulé, P., Duvernay, F., Boget, F., Chiavassa, T., 2008. Astron. Astrophys. 492, 719–724. https://doi.org/10.1051/0004-6361:200810536.
Bramble, M.S., Hand, K.P., 2024. Icarus 421, 116214. https://doi.org/10.1016/j.icarus.2024.116214.
Brown, R.H., Clark, R.N., Buratti, B.J., Cruikshank, D.P., Barnes, J.W., Mastrapa, R.M., Bauer, J., Newman, S., Momary, T., Baines, K.H., Bellucci, G., Capaccioni, F., Cerroni, P., Combes, M., Coradini, A., Drossart, P., Formisano, V., Jaumann, R., Langavin, Y., Matson, D.L., McCord, T.B., Nelson, R.M., Nicholson, P.D., Sicardy, B., Sotin, C., 2006. Science 311, 1425–1428. https://doi.org/10.1126/science.1121031.
Brucato, J.R., Baratta, G.A., Strazzulla, G., 2006. Astron. Astrophys. 455, 395–399. https://doi.org/10.1051/0004-6361:20065095.
Chaabouni, H., Schriver-Mazzuoli, L., Schriver, A., 2000. J. Phys. Chem. A 104, 6962–6969. https://doi.org/10.1021/jp0008290.
Chuang, K.J., Fedoseev, G., Qasim, D., Ioppolo, S., Jäger, C., Henning, T., Palumbo, M.E., Dishoeck, EF van, Linnartz, H., 2020. Astron. Astrophys. 635, A199. https://doi.org/10.1051/0004-6361/201937302.
Chuang, K.J., Fedoseev, G., Scirè, C., Baratta, G.A., Jäger, C., Henning, T., Linnartz, H., Palumbo, M.E., 2021. Astron. Astrophys. 650, A85. https://doi.org/10.1051/0004-6361/202140780.
Collings, M.P., Anderson, M.A., Chen, R., Dever, J.W., Viti, S., Williams, D.A., McCoustra, M.R.S., 2004. Mon. Not. Roy. Astron. Soc. 354, 1133–1140. https://doi.org/10.1111/j.1365-2966.2004.08272.x.
Combe, J.P., McCord, T.B., Matson, D.L., Johnson, T.V., Davies, A.G., Scipioni, F., Tosi, F., 2019. Icarus 317, 491–508. https://doi.org/10.1016/j.icarus.2018.08.007.
Cooper, J.F., 1983. J. Geophys. Res.: Space Phys. 88, 3945–3954. https://doi.org/10.1029/JA088iA05p03945.
Cooper, J.F., Cooper, P.D., Sittler, E.C., Sturner, S.J., Rymer, A.M., 2009. Planet. Space Sci. 57, 1607–1620. https://doi.org/10.1016/j.pss.2009.08.002.
de Barros, A.L.F., Bordalo, V., Duarte, E Seperuelo, da Silveira, E.F., Domaracka, A., Rothard, H., Boduch, P., 2011. Astron. Astrophys. 531, A160. https://doi.org/10.1051/0004-6361/201016021.
de Barros, A.L.F., da Silveira, E.F., Fulvio, D., Rothard, H., Boduch, P., 2016. Astrophys. J. 824, 81. https://doi.org/10.3847/0004-637X/824/2/81.
Ding, J.J., Boduch, P., Domaracka, A., Guillous, S., Langlinay, T., Lv, X.Y., Palumbo, M.E., Rothard, H., Strazzulla, G., 2013. Icarus 226, 860–864. https://doi.org/10.1016/j.icarus.2013.07.002.
d'Hendecourt, L.B., Allamandola, L.J., 1986. Astron. AstroPhys. Suppl. 64, 453–467.
Emery, J.P., Burr, D.M., Cruikshank, D.P., Brown, R.H., Dalton, J.B., 2005. Astron. Astrophys. 435, 353–362. https://doi.org/10.1051/0004-6361:20042482.
Ferus, M., Nesvorný, D., Šponer, J., Kubelík, P., Michalčikova, R., Shestivská, V., Šponer, J.E., Civiš, S., 2015. Proceedings Natl. Acad. Sci. USA 112, 657–662. https://doi.org/10.1073/pnas.1412072111.
Franchi, F., Túri, M., Lakatos, G., Rahul, K.K., Mifsud, D.V., Panieri, G., Rácz, R., Kovács, S.T.S., Furu, E., Huszánk, R., McCullough, R.W., Juhász, Z., 2025. Planet. Space Sci. 257, 106051. https://doi.org/10.1016/j.pss.2025.106051.
Frasco, D.L., 1964. J. Chem. Phys. 41, 2134–2140. https://doi.org/10.1063/1.1726217.
Gerakines, P.A., Hudson, R.L., 2015a. Astrophys. J. Lett. 805, L20. https://doi.org/10.1088/2041-8205/805/2/L20.
Gerakines, P.A., Hudson, R.L., 2015b. Astrophys. J. Lett. 808, L40. https://doi.org/10.1088/2041-8205/808/2/L40.
Gerakines, P.A., Schutte, W.A., Greenberg, J.M., van Dishoeck, E.F., 1995. Astron. Astrophys. 296, 810–818.
Gerakines, P.A., Materese, C.K., Hudson, R.L., 2023. Mon. Not. Roy. Astron. Soc. 522, 3145–3162. https://doi.org/10.1093/mnras/stad1164.
Hagen, W., Tielens, A.G.G.M., Greenberg, J.M., 1981. Chem. Phys. 1981, 367–379. https://doi.org/10.1016/0301-0104(81)80158-9.
Hand, K.P., Carlson, R.W., 2011. Icarus 215, 226–233. https://doi.org/10.1016/j.icarus.2011.06.031.
Hendrix, A.R., House, C.H., 2023. Commun. Earth Environ. 4, 485. https://doi.org/10.1038/s43247-023-01130-8.
Hendrix, A.R., Hansen, C.J., Holsclaw, G.M., 2010. Icarus 206, 608–617. https://doi.org/10.1016/j.icarus.2009.11.007.
Hodyss, R., Johnson, P.V., Stern, J.V., Goguen, J.D., Kanik, I., 2009. Icarus 200, 338–342. https://doi.org/10.1016/j.icarus.2008.10.024.
Howett, C., Hendrix, A.R., Nordheim, T., Paranicas, C., Spencer, J., Verbiscer, A., 2018. Ring and magnetosphere interactions with satellite surfaces. In: Enceladus and the Icy Moons of Saturn. University of Arizona Press, Tucson AZ, pp. 343–360.
Hsu, H.W., Postberg, F., Sekine, Y., Shibuya, T., Kempf, S., Horányi, M., Juhász, A., Altobelli, N., Suzuki, K., Masaki, Y., Kuwatini, T., Tachibana, S., Sirono, S.I., Moragas-Klostermeyer, G., Srama, R., 2015. Nature 519, 207–210. https://doi.org/10.1038/nature14262.
Hudson, R.L., 2017. Spectrochim. Acta: Mol. Biomol. Spectrosc. 187, 82–86. https://doi.org/10.1016/j.saa.2017.06.027.
Hudson, R.L., Ferrante, R.F., 2020. Mon. Not. Roy. Astron. Soc. 492, 283–293. https://doi.org/10.1093/mnras/stz3323.
Hudson, R.L., Loeffler, M.J., 2013. Astrophys. J. 773, 109. https://doi.org/10.1088/0004-637X/773/2/109.
Hudson, R.L., Moore, M.H., Gerakines, P.A., 2001. Astrophys. J. 550, 1140. https://doi.org/10.1086/319799.
Hudson, R.L., Ferrante, R.F., Moore, M.H., 2014. Icarus 228, 276–287. https://doi.org/10.1016/j.icarus.2013.08.029.
Hudson, R.L., Gerakines, P.A., Yarnall, Y.Y., 2022. Astrophys. J. 925, 156. https://doi.org/10.3847/1538-4357/ac3e74.
Hudson, R.L., Gerakines, P.A., Yarnall, Y.Y., 2024. Astrophys. J. 970, 108. https://doi.org/10.3847/1538-4357/ad47a5.
Ip, W.H., 2000. Planet. Space Sci. 48, 775–783. https://doi.org/10.1016/S0032-0633(00)00036-2.

Islam, F., Baratta, G.A., Palumbo, M.E., 2014. Astron. Astrophys. 561, A73. https://doi.org/10.1051/0004-6361/201322010.
Jacox, M.E., Milligan, D.E., 1973. J. Mol. Spectrosc. 47, 148–162. https://doi.org/10.1016/0022-2852(73)90084-2.
James, R.L., Ioppolo, S., Hoffmann, S.V., Jones, N.C., Mason, N.J., Dawes, A., 2020. RSC Adv. 10, 37515–37528. https://doi.org/10.1039/d0ra05826b.
James, R.L., Ioppolo, S., Hoffmann, S.V., Jones, N.C., Mason, N.J., Dawes, A., 2021. RSC Adv. 11, 33055–33069. https://doi.org/10.1039/d1ra05600j.
Jaumann, R., Stephan, K., Hansen, G.B., Clark, R.N., Buratti, B.J., Brown, R.H., Baines, K. H., Newman, S.F., Bellucci, G., Filacchione, G., Coradini, A., Cruikshank, D.P., Griffith, C.A., Hibbitts, C.A., McCord, T.B., Nelson, R.M., Nicholson, P.D., Sotin, C., Wagner, R., 2008. Icarus 193, 407–419. https://doi.org/10.1016/j.icarus.2007.09.013.
Jheeta, S., Ptasinska, S., Sivaraman, B., Mason, N.J., 2012. Chem. Phys. Lett. 543, 208–212. https://doi.org/10.1016/j.cplett.2012.06.051.
Johnson, R.E., Famá, M., Liu, M., Baragiola, R.A., Sittler, E.C., Smith, H.T., 2008. Planet. Space Sci. 56, 1238–1243. https://doi.org/10.1016/j.pss.2008.04.003.
Jones, B.M., Bennett, C.J., Kaiser, R.I., 2011. Astrophys. J. 734, 78. https://doi.org/10.1088/0004-637X/734/2/78.
Kempf, S., Beckmann, U., Schmidt, J., 2010. Icarus 206, 446–457. https://doi.org/10.1016/j.icarus.2009.09.016.
Khanna, R.K., Moore, M.H., 1999. Spectrochim. Acta: Mol. Biomol. Spectrosc. 55, 961–967. https://doi.org/10.1016/s1386-1425(98)00228-5.
Loeffler, M.J., Baratta, G.A., Palumbo, M.E., Strazzulla, G., Baragiola, R.A., 2005. Astron. Astrophys. 435, 587–594. https://doi.org/10.1051/0004-6361:20042256.
López-Sepulcre, A., Balucani, N., Ceccarelli, C., Codella, C., Dulieu, F., Theulé, P., 2019. ACS Earth Space Chem. 3, 2122–2137. https://doi.org/10.1021/acsearthspacechem.9b00154.
MacKenzie, S.M., Neveu, M., Davila, A.F., Lunine, J.I., Craft, K.L., Cable, M.L., Phillips-Lander, C.M., Hofgartner, J.D., Eigenbrode, J.L., Waite, J.H., Glein, C.R., Gold, R., Greenauer, P.J., Kirby, K., Bradburne, C., Kounaves, S.P., Malaska, M.J., Postberg, F., Patterson, G.W., Porco, C., Núñez, J.I., German, C., Huber, J.A., McKay, C.P., De Vera, J.P., Brucato, J.R., Spilker, L.J., 2021. Planet. Sci. J. 2, 77. https://doi.org/10.3847/psj/abe4da.
Marks, J.H., Wang, J., Sun, B.J., McAnally, M., Turner, A.M., Chang, A.H.H., Kaiser, R.I., 2023. ACS Cent. Sci. 9, 2241–2250. https://doi.org/10.1021/acscentsci.3c01108.
Martín-Doménech, R., Manzano-Santamaría, J., Muñoz-Caro, G.M., Cruz-Díaz, G.A., Chen, Y.J., Herrero, V.J., Tanarro, I., 2015. Astron. Astrophys. 584, A14. https://doi.org/10.1051/0004-6361/201526003.
Martins, Z., Bunce, E., Grasset, O., Hamp, R., Jones, G., Le Gall, A., Lucchetti, A., Postberg, F., Prieto-Ballesteros, O., Roth, L., Tortora, P., Vorburger, A., 2024. Report of the Expert Committee for the Large-Class Mission in Esa's Voyage 2050 Plan Covering the Science Theme *Moons of the Giant Planets*. European Space Agency. Technical Report.
Mejía, C., de Barros, A.L.F., Rothard, H., Boduch, P., da Silveira, E.F., 2020. Astrophys. J. 894, 132. https://doi.org/10.3847/1538-4357/ab8935.
Mifsud, D.V., Kaňuchová, Z., Ioppolo, S., Herczku, P., Traspas Muiña, A., Field, T.A., Hailey, P.A., Juhász, Z., Kovács, S.T.S., Mason, N.J., McCullough, R.W., Pavithraa, S., Rahul, K.K., Paripás, B., Sulik, B., Chou, S.L., Lo, J.I., Das, A., Cheng, B. M., Rajasekhar, B.N., Bhardwaj, A., Sivaraman, B., 2022. J. Mol. Spectrosc. 385, 111599. https://doi.org/10.1016/j.jms.2022.111599.
Mifsud, D.V., Herczku, P., Rahul, K.K., Ramachandran, R., Sundararajan, P., Kovács, S.T. S., Sulik, B., Juhász, Z., Rácz, R., Biri, S., Kaňuchová, Z., McCullough, R.W., Sivaraman, B., Ioppolo, S., Mason, N.J., 2023a. Phys. Chem. Chem. Phys. 25, 26278–26288. https://doi.org/10.1039/d3cp03196a.
Mifsud, D.V., Herczku, P., Sulik, B., Juhász, Z., Vajda, I., Rajta, I., Ioppolo, S., Mason, N. J., Strazzulla, G., Kaňuchová, Z., 2023b. Atoms 11 (19). https://doi.org/10.3390/atoms11020019.
Mifsud, D.V., Herczku, P., Ramachandran, R., Sundararajan, P., Rahul, K.K., Kovács, S.T. S., Sulik, B., Juhász, Z., Rácz, R., Biri, S., Kaňuchová, Z., Ioppolo, S., Sivaraman, B., McCullough, R.W., Mason, N.J., 2024. Spectrochim. Acta: Mol. Biomol. Spectrosc. 319, 124567. https://doi.org/10.1016/j.saa.2024.124567.
Moon, E.S., Kang, H., Oba, Y., Watanabe, N., Kouchi, A., 2010. Astrophys. J. 713, 906–911. https://doi.org/10.1088/0004-637X/713/2/906.
Moore, M.H., Hudson, R.L., 1998. Icarus 135, 518–527. https://doi.org/10.1006/icar.1998.5996.
Moore, M.H., Ferrante, R.F., Hudson, R.L., Stone, J.N., 2007. Icarus 190, 260–273. https://doi.org/10.1016/j.icarus.2007.02.020.
Morooka, M.W., Wahlund, J.E., Eriksson, A.I., Farrell, W.M., Gurnett, D.A., Kurth, W.S., Persoon, A.M., Shafiq, M., André, M., Holmberg, M.K., 2011. J. Geophys. Res.: Space Phys. 116, 12221. https://doi.org/10.1029/2011ja017038.
Morris, S.M., 1992. Annu. Rev. Nutr. 12, 81–101.
Mousis, O., Bouquet, A., Langevin, Y., André, N., Boithias, H., Durry, G., Faye, F., Hartogh, P., Helbert, J., Iess, L., Kempf, S., Masters, A., Postberg, F., Renard, J.B., Vernazza, P., Vorburger, A., Wurz, P., Atkinson, D.H., Barabash, S., Berthomier, M., Brucato, J., Cable, M., Carter, J., Cazaux, S., Coustenis, A., Danger, G., Dehant, V., Fornaro, T., Garnier, P., Guatier, T., Groussin, O., Hadid, L.Z., Ize, J.C., Kolmasova, I., Lebreton, J.P., Le Maistre, S., Lellouch, E., Lunine, J.I., Mandt, K.E., Martins, Z., Mimoun, D., Nenon, Q., Muñoz Caro, G.M., Rannou, P., Rauer, H., Schmitt-Kopplin, P., Schneeberger, A., Simons, M., Stephen, K., Van Hoolst, T., Vaverka, J., Wieser, M., Wörner, L., 2022. Planet. Sci. J. 3, 268. https://doi.org/10.3847/PSJ/ac9c03.
Muñoz-Caro, G.M., Dartois, E., Boduch, P., Rothard, H., Domaracka, A., Jiménez-Escobar, A., 2014. Astron. Astrophys. 566, A93. https://doi.org/10.1051/0004-6361/201322983.
Muntean, E.A., Lacerda, P., Field, T.A., Fitzsimmons, A., Hunniford, C.A., McCullough, R. W., 2015. Surf. Sci. 641, 204–209. https://doi.org/10.1016/j.susc.2015.07.005.
Newman, S.F., Buratti, B.J., Brown, R.H., Jaumann, R., Bauer, J., Momary, T., 2008. Icarus 193 (2), 397–406. https://doi.org/10.1016/j.icarus.2007.04.019.
Paranicas, C., Mitchell, D.G., Krimigis, S.M., Hamilton, D.C., Roussos, E., Krupp, N., Jones, G.H., Johnson, R.E., Cooper, J.F., Armstrong, T.P., 2008. Icarus 197 (2), 519–525. https://doi.org/10.1016/j.icarus.2008.05.011.
Paranicas, C., Roussos, E., Decker, R.B., Johnson, R.E., Hendrix, A.R., Schenk, P., Cassidy, T.A., Dalton, J.B., Howett, C.J., Kollmann, P., Patterson, W., Hand, K.P., Nordheim, T.A., Krupp, N., Mitchell, D.G., 2014. Icarus 234, 155–161. https://doi.org/10.1016/j.icarus.2014.02.026.
Pearl, J., Ngoh, M., Ospina, M., Khanna, R., 1991. J. Geophys. Res.: Planets 96, 17477–17482. https://doi.org/10.1029/91JE01741.
Persoon, A.M., Gurnett, D.A., Leisner, J.S., Kurth, W.S., Groene, J.B., Faden, J.B., 2013. J. Geophys. Res.: Space Phys. 118, 2970–2974. https://doi.org/10.1002/jgra.50182.
Peter, J.S., Nordheim, T.A., Hand, K.P., 2024. Nat. Astron. 8, 164–173. https://doi.org/10.1038/s41550-023-02160-0.
Porco, C.C., Helfenstein, P., Thomas, P.C., Ingersoll, A.P., Wisdom, J., West, R., Neukum, G., Denk, T., Wagner, R., Roatsch, T., Kieffer, S., Turtle, E., McEwen, A., Johnson, T.V., Rathbun, J., Veverka, J., Wilson, D., Perry, J., Spitale, J., Brahic, A., Burns, J.A., Delgenio, A.D., Dones, L., Murray, C.D., Squyres, S., 2006. Science 311, 1393–1401. https://doi.org/10.1126/science.1123013.
Postberg, F., Khawaja, N., Abel, B., Choblet, G., Glein, C.R., Gudipati, M.S., Henderson, B. L., Hsu, H.W., Kempf, S., Klenner, F., Moragas-Klostermeyer, G., Magee, B., Nölle, L., Perry, M., Reviol, R., Schmidt, J., Srama, R., Stolz, F., Tobie, G., Trieloff, M., Waite, J.H., 2018. Nature 558, 564–568. https://doi.org/10.1038/s41586-018-0246-4.
Potapov, A., Jäger, C., Henning, T., 2020. Astrophys. J. 894, 110. https://doi.org/10.3847/1538-4357/ab86b5.
Rachid, M.G., Pilling, S., Rocha, W.R.M., Agnihotri, A., Rothard, H., Boduch, P., 2020. Mon. Not. Roy. Astron. Soc. 494, 2396–2409. https://doi.org/10.1093/mnras/staa778.
Rácz, R., Kovács, S.T.S., Lakatos, G., Rahul, K.K., Mifsud, D.V., Herczku, P., Sulik, B., Juhász, Z., Perduk, Z., Ioppolo, S., Mason, N.J., Field, T.A., Biri, S., McCullough, R. W., 2024. Rev. Sci. Instrum. 95, 095105. https://doi.org/10.1063/5.0207967.
Raut, U., Baragiola, R.A., 2013. Astrophys. J. 772, 53. https://doi.org/10.1088/0004-637X/772/53.
Robidel, R., Le Mouélic, S., Tobie, G., Massé, M., Seignovert, B., Sotin, C., Rodriguez, S., 2020. Icarus 349, 113848. https://doi.org/10.1016/j.icarus.2020.113848.
Sakai, S., Cravens, T.E., Omidi, N., Perry, M.E., Waite, J.H., 2016. Planet. Space Sci. 130, 60–79. https://doi.org/10.1016/j.pss.2016.05.007.
Saladino, R., Crestini, C., Pino, S., Costanzo, G., Di Mauro, E., 2012. Phys. Life Rev. 9, 84–104. https://doi.org/10.1016/j.plrev.2011.12.002.
Sharma, H., Hedman, M.M., Vahidinia, S., 2023. Planet. Sci. J. 4, 108. https://doi.org/10.3847/psj/acd5d4.
Sivaraman, B., Rajasekhar, B.N., Nair, B.G., Hatode, V., Mason, N.J., 2013. Spectrochim. Acta: Mol. Biomol. Spectrosc. 105, 238–244. https://doi.org/10.1016/j.saa.2012.12.039.
Smith, H.T., Crary, F.J., Dougherty, M.K., Perry, M.E., Roussos, E., Simon, S., Tokar, R.L., 2018. Enceladus and its influence on saturn's magnetosphere. In: Enceladus and the Icy Moons of Saturn. University of Arizona Press, Tucson AZ, pp. 212–231.
Southworth, B., Kempf, S., Spitale, J., 2018. Icarus 319, 33–42. https://doi.org/10.1016/j.icarus.2018.08.024.
Spencer, J.R., Nimmo, F., 2013. Annu. Rev. Earth Planet Sci. 41, 693–717. https://doi.org/10.1146/annurev-earth-050212-124025.
Spencer, J.R., Pearl, J.C., Segura, M., Flasar, F.M., Mamoutkine, A., Romani, P., Buratti, B.J., Hendrix, A.R., Spilker, L.J., Lopes, R.M., 2006. Science 311, 1401–1405. https://doi.org/10.1126/science.1121661.
Spencer, J.R., Barr, A.C., Esposito, L.W., Helfenstein, P., Ingersoll, A.P., Jaumann, R., McKay, C.P., Nimmo, F., Waite, J.H., 2009. Enceladus: an active cryovolcanic satellite. In: Saturn from Cassini-Huygens. Springer, Dordrecht, pp. 683–724.
Strazzulla, G., Palumbo, M.E., 1998. Planet. Space Sci. 46, 1339–1348. https://doi.org/10.1016/S0032-0633(97)00210-9.
Terwisscha van Scheltinga, J., Ligterink, N.F.W., Boogert, A.C.A., van Dishoeck, E.F., Linnartz, H., 2018. Astron. Astrophys. 611, A35. https://doi.org/10.1051/0004-6361/201731998.
Thomsen, M.F., Van Allen, J.A., 1980. J. Geophys. Res.: Space Phys. 85, 5831–5834. https://doi.org/10.1029/JA085iA11p05831.
Tokar, R.L., Wilson, R.J., Johnson, J.E., Henderson, M.G., Thomsen, M.F., Cowee, M.M., Sittler, J.C., Young, D.T., Crary, F.J., McAndrews, H.J., Smith, H.T., 2008. Geophys. Res. Lett. 35, L14202. https://doi.org/10.1029/2008gl034749.
Tokar, R.L., Johnson, R.E., Thomsen, M.F., Wilson, R.J., Young, D.T., Crary, F.J., Coates, A.J., Jones, G.H., Paty, C.S., 2009. Geophys. Res. Lett. 36, L13203. https://doi.org/10.1029/2009gl038923.
van Broekhuizen, F.A., Keane, J.V., Schutte, W.A., 2004. Astron. Astrophys. 415, 425–436. https://doi.org/10.1051/0004-6361:20034161.
Vasconcelos, F.A., Pilling, S., Rocha, W.R.M., Rothard, H., Boduch, P., Ding, J.J., 2017. Phys. Chem. Chem. Phys. 19, 12845–12856. https://doi.org/10.1039/c7cp00883j.
Villanueva, G.L., Hammel, H.B., Milam, S.N., Kofman, V., Faggi, S., Glein, C.R., Cartwright, R., Roth, L., Hand, K.P., Paganini, L., Spencer, J., Stansberry, J., Holler, B., Rowe-Gurney, N., Protopapa, S., Strazzulla, G., Liuzzi, G., Cruz-Mermy, G., El Moutamid, M., Hedman, M., Denny, K., 2023. Nat. Astron. 7, 1056–1062. https://doi.org/10.1038/s41550-023-02009-6.
Waite, J.H., Glein, C.R., Perryman, R.S., Teolis, B.D., Magee, B.A., Miller, G., Grimes, J., Perry, M.E., Miller, K.E., Bouquet, A., Lunine, J.I., Brockwell, T., Bolton, S.J., 2017. Science 356, 155–159. https://doi.org/10.1126/science.aai8703.

Young, D.T., Berthelier, J.J., Blanc, M., Burch, J.L., Bolton, S., Coates, A.J., Crary, F.J., Goldstein, R., Grande, M., Hill, T.W., Johnson, R.E., Baragiola, R.A., Kelha, V., McComas, D.J., Mursula, K., Sittler, E.C., Svenes, K.R., Szegö, K., Tanskanen, P., Thomsen, M.F., Bakshi, S., Barraclough, B.L., Bebesi, Z., Delapp, D., Dunlop, M.W., Gosling, J.T., Furman, J.D., Gilbert, L.K., Glenn, D., Holmlund, C., Illiano, J.M., Lewis, G.R., Linder, D.R., Maurice, S., McAndrews, H.J., Narheim, B.T., Pallier, E., Reisenfeld, D., Rymer, A.M., Smith, H.T., Tokar, R.L., Vilppola, J., Zinsmeyer, C., 2005. Science 307, 1262–1266. https://doi.org/10.1126/science.1106151.

Zeiss, H.H., Tsutui, M., 1953. J. Am. Chem. Soc. 75, 897–900. https://doi.org/10.1021/ja01100a036.

Ziegler, J.F., Ziegler, M.D., Biersack, J.P., 2010. Nucl. Instrum. Methods Phys Res. B: Beam Interactions with Mater. Atoms 268, 1818–1823. https://doi.org/10.1016/j.nimb.2010.02.091.